Available online at www.sciencedirect.com
ScienceDirect
Journal of Nuclear Materials 367–370 (2007) 742–747
journal of nuclear materials
www.elsevier.com/locate/jnucmat

Swelling and time-dependent crack growth in SiC/SiC composites

Charles H. Henager Jr. *

Pacific Northwest National Laboratory, 902 Battelle Boulevard, MS: P8-15, Richland, WA 99352-0999, USA

Abstract

SiC continuous-fiber composites are considered for nuclear applications but concern has centered on the differential materials response of the fiber, fiber/matrix interphase (fiber coating), and matrix. In our study, a continuous-fiber composite is simulated by four concentric cylinders to explore the magnitude of radial stresses when irradiation swelling of the various components is incorporated. The outputs of this model were input into a time-dependent crack-bridging model to predict crack growth rates in an environment where thermal and irradiation creep of SiC-based fibers is considered. Under assumed Coulomb friction the fiber–matrix sliding stress decreases with increasing dose and then increases once the pyrocarbon swelling reaches 'turn around'. This causes an initial increase in crack growth rate and higher stresses in crack bridging fibers at higher doses. An assumed irradiation creep law for fine-grained SiC fibers is shown to dominate the radiation response.

1. Introduction

SiC-based continuous-fiber composites are considered for nuclear applications as structural components, but concern has centered on the differential materials response of the fiber, pyrocarbon fiber/matrix interphase (fiber coating), and matrix under irradiation [1]. A modeling approach using concentric cylindrical regions to simulate continuous-fiber composites to give the stress distribution in each region was developed to explore thermo-mechanical loading effects [2–5]. This model provided an elastic solution to the fiber, fiber–matrix interphase, matrix, and far-field composite regions for thermo-mechanical strains and irradiation-induced strains as a functions of temperature and neutron dose [5]. The influence of pyrocarbon density on swelling was shown to determine the radial stress present at the fiber–matrix interface as a function of dose for composites containing stoichiometric SiC fibers, which can ultimately influence composite mechanical properties through the frictional sliding stress, τ.

Time-dependent, and thus dose-dependent, properties of interest for SiC-composites include retained strength, dimensional stability, and creep-crack growth [1], which have been addressed partly by a dynamic crack growth model developed to predict SiC-composite lifetimes [6–8]. However, crack growth models have omitted dose-dependent swelling until the development of the modified four-cylinder model.

* Tel.: +1 509 376 1442; fax: +1 509 376 0418.
E-mail address: chuck.henager@pnl.gov

0022-3115/$ - see front matter
doi:10.1016/j.jnucmat.2007.03.088

The synthesis of these two models will afford a more detailed understanding and, hopefully, improved predictive capabilities with respect to dose-dependent mechanical properties of SiC-composites.

2. Simulation details

2.1. Four-cylinder model

A continuous-fiber composite is simulated by four concentric cylinders [3] as shown in Fig. 1, with each cylinder considered a distinct material region numbered 1–4 starting from the outermost cylinder as region 1. The surrounding composite is the outermost cylinder, region 1, while the matrix, fiber coating, and fiber are the remaining cylinders, with the fiber being the innermost cylinder, region 4. The cylinders are subject to three independent boundary conditions; axisymmetric temperature change, $\Delta T(r)$, uniaxial applied stress, σ_{oz}, and biaxial applied stress, σ_{or}, where r and z are the radial and axial components referred to cylindrical coordinates (r, θ, z). Stress relaxation was not allowed during irradiation or during cooling from the fabrication temperature and all components remain elastic and perfectly bonded. The fiber, matrix, and surrounding composite were treated as isotropic materials, while the pyrocarbon coatings were considered to be transversely isotropic [2]. The elastic solution gives the axial, radial, hoop stress in all the regions ($n = 1, 2, 3, 4$) as

$$\sigma_r^n = C_{11}^n\left(A_n - \frac{B_n}{r^n}\right) + C_{12}^n\left(A_n + \frac{B_n}{r^n}\right) + C_{13}^n E_n - \beta_1^n \Delta T - \gamma_1^n, \tag{1a}$$

$$\sigma_\theta^n = C_{12}^n\left(A_n - \frac{B_n}{r^n}\right) + C_{11}^n\left(A_n + \frac{B_n}{r^n}\right) + C_{13}^n E_n - \beta_1^n \Delta T - \gamma_1^n, \tag{1b}$$

$$\sigma_z^n = 2C_{13}^n A_n + C_{33}^n E_n - \beta_3^n \Delta T - \gamma_3^n, \tag{1c}$$

where C_{ij}^n are the material elastic properties, ΔT is the uniform temperature change, and A_n, B_n, and E_n are the coefficients of the solutions of the four cylinder problem for the appropriate boundary conditions [2,3]. For this problem, $B_4 = 0$ and $E_n = E$ for all n. The terms involving β_i are defined as

$$\beta_1^n = (C_{11}^n + C_{12}^n)\alpha_{\mathrm{T}}^n + C_{13}^n \alpha_{\mathrm{L}}^n; \quad \beta_3^n = 2C_{12}^n \alpha_{\mathrm{T}}^n + C_{33}^n \alpha_{\mathrm{L}}^n, \tag{2}$$

where α_{T} and α_{L} are the transverse (T) and longitudinal (L) coefficients of thermal expansion for each domain. Transverse refers to in-plane properties and longitudinal refers to properties parallel to the z-axis. The γ_i terms are defined in each domain as the radiation-induced stresses as

$$\gamma_1^n = (C_{11}^n + C_{12}^n)\varepsilon_{\mathrm{T}}^n + C_{13}^n \varepsilon_{\mathrm{L}}^n; \quad \gamma_3^n = 2C_{12}^n \varepsilon_T^n + C_{33}^n \varepsilon_{\mathrm{L}}^n. \tag{3}$$

The ε_{T} and ε_{L} terms are determined from swelling data for each material in the composite.

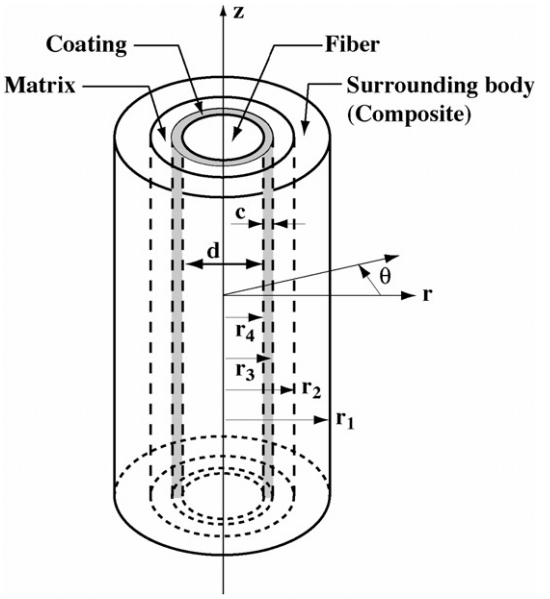

Fig. 1. Schematic of four-cylinder model showing coordinate system and identifying the four regions. Fiber has diameter d and the coating has thickness c and the remaining radii are computed from the fiber volume fraction.

2.2. Dose-dependent sliding stress

The data of Kaae [9] was used to provide swelling data for three pyrolytic carbons as a function of fast-neutron fluence. Irradiations were performed in HFIR-PTP, where the spectrally averaged dpa cross-section is 158 barns and the damage rate is 28 dpa/efpy (effective full power year) or 1.4×10^{23} total n/cm^2/efpy [10]. The experimental results were reported in [9] as a function of dose in units of 10^{25} n/m^2 for $E > 29$ fJ (or 0.18 MeV). Conversion to dose in dpa was accomplished by determining the fraction of neutrons with $E >$ 0.18 MeV to be 0.23, then the dose conversion factor is 10^{25} n/m^2, $E > 29$ fJ, is equivalent to 0.87 dpa.

These curves are shown in Fig. 2 for two types of pyrocarbon, denoted as high-density isotropic carbon (HDIC) and low-density isotropic carbon (LDIC) [9]. Using the material constants listed in

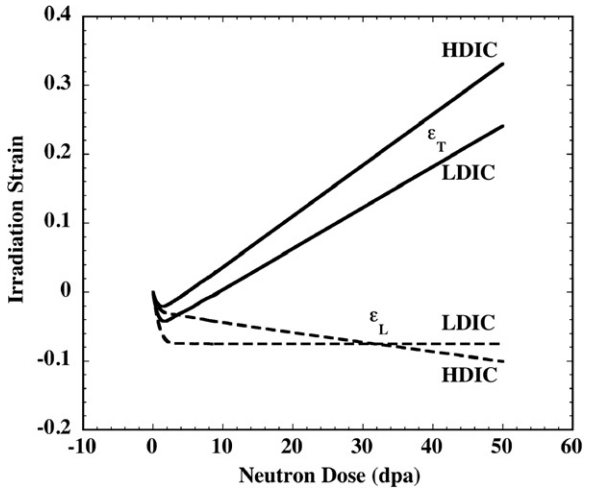

Fig. 2. Longitudinal and transverse radiation-induced strain as a function of neutron dose in dpa for two types of pyrolytic carbon used as typical fiber coatings (HDIC and LDIC).

Table 1, the four-cylinder model predictions for the radial stress as a function of dose and pyrocarbon type are shown in Fig. 3(a) for an assumed 100 nm-thick pyrocarbon layer. The radial stress that develops as a function of dose is a quantity at the individual fiber level that can influence composite mechanical properties through changes in the frictional sliding stress. Assuming that the material obeys Coulomb's friction law, the frictional sliding stress can be related to the radial stress as

$$\tau = -\mu\sigma_{rr}, \tag{4}$$

where τ is the frictional sliding stress, μ is the coefficient of friction at the fiber–matrix interface due to the pyrocarbon interphase, and σ_{rr} is the radial stress. This equation connects the output of the four-cylinder model with fiber bridging mechanics, and the sliding stress as a function of dose is shown in Fig. 3(b) for an assumed range for the coefficient of friction, $\mu = 0.05$, 0.1, or 0.2 [11,12]. This data provides an additional dose-dependent parameter for our dynamic crack growth model.

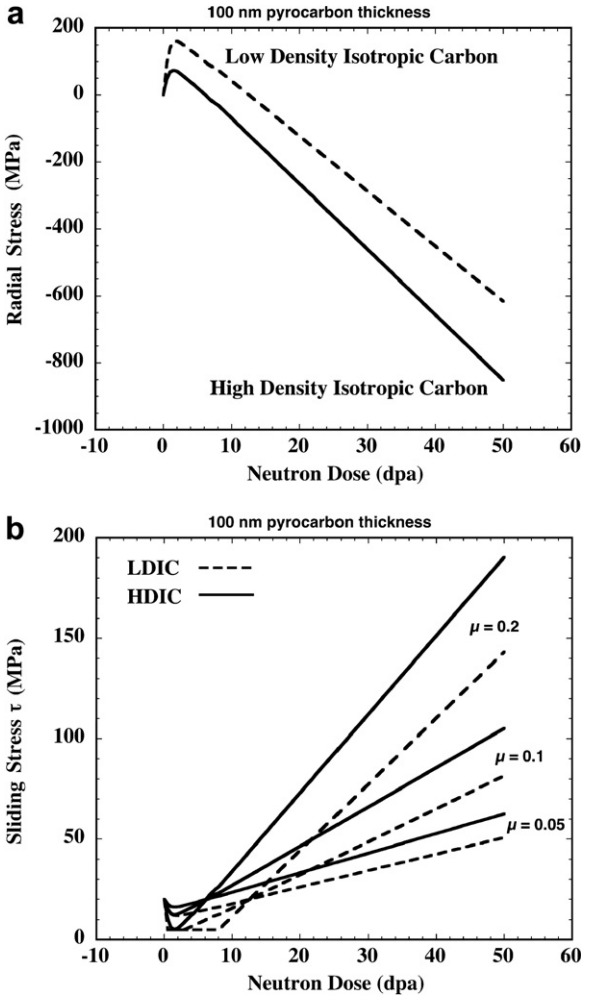

Fig. 3. Predicted (a) radial and (b) sliding stresses at fiber–matrix interface for Type-S fiber composites with the indicated carbon coating of 100 nm subjected to neutron irradiation at 1273 K and with the assumed coefficients of friction as indicated.

2.3. Dynamic crack growth model

A 2D dynamic crack growth model has been developed at Pacific Northwest National Laboratory (PNNL) based on subcritical crack growth

Table 1
Properties used in calculations

Materials	Young's modulus (GPa)		Poisson's ratio		CTE (10^{-6} C^{-1})	
	Axial, E_L	Transverse, E_T	Axial, ν_L	In-plane, ν_T	Axial, α_L	Transverse, α_L
Type-S SiC fiber [17]	420	420	0.2	0.2	4.0	4.0
SiC matrix [18]	460	460	0.22	0.22	4.5	4.5
HDIC[a] [9]	80	80	0.23	0.23	5	5
LDIC[b] [9]	80	80	0.23	0.23	5	5

[a] High-density isotropic carbon.
[b] Low-density isotropic carbon.

Table 2
Fiber creep parameters

Fiber type and condition	Creep law[a]	A ($MPa^{-1}\,s^{-1}$)	K ($MPa^{-1}\,dpa^{-1}$)	n	p	Q (kJ/mol)
Type-S thermal	$\varepsilon = A\sigma^n t^p \mathrm{Exp}\left(\frac{-Qp}{RT}\right)$	0.0667		1.4	0.61	425
Sylramic irradiation	$\varepsilon = K\dot{\phi}\sigma t$		4.7×10^{-6}	–	–	50

[a] σ is stress in MPa, t is time in seconds, Q is activation energy in kJ/mol, A is a constant, and K is irradiation creep compliance for Sylramic fibers. Constants n and p are stress and time-temperature exponents, respectively.

experiments on SiC/SiC composites at elevated temperatures [13–15]. Once a relationship between crack-opening displacement and bridging tractions from crack-bridging elements is determined, a governing integral equation is obtained that relates the total crack opening, and the bridging tractions, to the applied load. The solution of this equation gives the force on the crack-bridges and the crack-opening displacement everywhere along the crack face [7]. This relation is rendered time-dependent by including appropriate bridging fiber creep laws. For fusion environments, both thermal and irradiation-induced fiber creep are included. Since the frictional sliding stress, τ, is an input parameter for this dynamic model, the results given in this paper allow τ to be dose-dependent, which can modify the resultant fiber bridging mechanics.

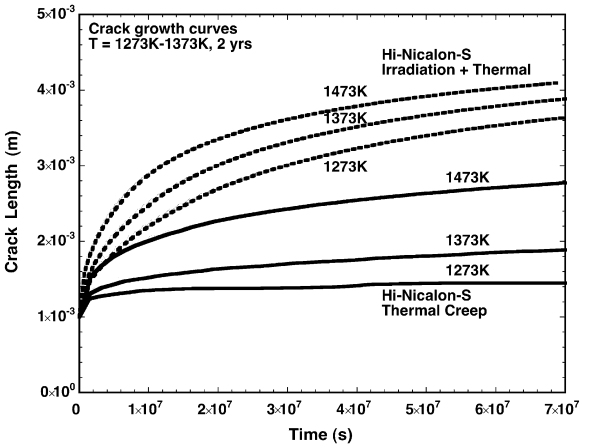

Fig. 4. Crack growth curves due to fiber thermal creep only (solid lines) or thermal plus radiation-induced creep (dashed lines) at 1273–1473 K.

3. Results and discussion

Several different cases were studied under simulated neutron irradiation at 1273–1473 K using a dose rate of 10 dpa/year for a SiC-composite with SiC Type-S fibers. Time-dependent crack growth considering both thermal and thermal plus radiation-induced fiber creep was modeled using a dose-independent sliding stress. This was compared to model predictions using the variable sliding stress results. Values of the domain radii for the four-cylinder model were chosen to match microstructural information for CVI SiC/SiC composites. The fiber coating thickness was 100 nm, which is representative of pyrocarbon thicknesses. The stresses were computed out to 20 dpa, or 2 years of irradiation.

3.1. Crack growth due to fiber creep with constant sliding stress

Fiber thermal creep parameters for Hi-Nicalon Type-S SiC fibers were obtained from DiCarlo et al.,[1] while radiation-induced creep parameters were obtained from the work of Scholz and Youngblood [16] for Sylramic SiC fibers, which is a fine-grained SiC fiber comparable to the Type-S fiber. These creep parameters are shown in Table 2. The dynamic crack growth model reveals that Hi-Nicalon Type-S composites are thermal-creep resistant at 1273 K but that using the assumed radiation-induced fiber creep law results in high crack growth rates, where the radiation-induced fiber creep is the dominant deformation mechanism. These crack growth results are shown in Fig. 4 for a composite bar in four-point bending at 1273–1473 K with an assumed crack in the bar loaded to 10 $MPa\sqrt{m}$ and with an initial sliding stress of 20 MPa.

3.2. Crack growth with variable sliding stress

The sliding stress is then allowed to vary according to Fig. 3(b) for both HDIC and LDIC pyrocarbon interfaces of 100-nm thickness and for the assumed friction coefficients. For both pyrocarbon materials there is a dose at which 'turn around' occurs in their swelling and growth curves. Initially there is densification of the pyrocarbon and net radial shrinkage, which acts to reduce the sliding

[1] Private communication from J.A. DiCarlo, NASA Glenn Research, James.A.DiCarlo@nasa.gov.

stress. At 'turn around' pyrocarbon shrinkage stops and net radial swelling begins, which acts to put the fiber–matrix interface into compression and increase the sliding stress according to Eq. (4). The sliding stress, τ, is assumed to be 20 MPa at $t = 0$ and decreases with increasing tensile σ_{rr} but τ is not allowed to decrease below 5 MPa. This lower bound value for τ is chosen arbitrarily but fiber surface roughness effects are thought to prevent τ from completely vanishing even if debonding occurs at the fiber–matrix interface due to swelling. These predicted crack growth curves are shown in Fig. 5. Crack growth is initially more rapid compared to the constant sliding stress case when this detail is included, but then begins to decrease after 'turn around' as the sliding stress begins to increase with increasing dose.

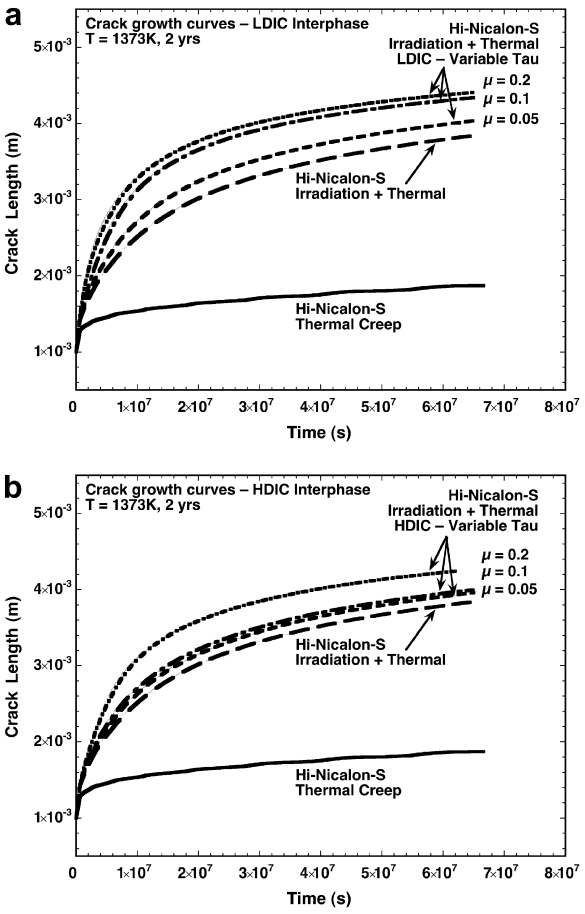

Fig. 5. Crack length as a function of time showing the effects of including a dose-dependent sliding stress in the dynamic crack modeling at 1373 K for (a) LDIC interphase and (b) HDIC interphase and indicated friction coefficient.

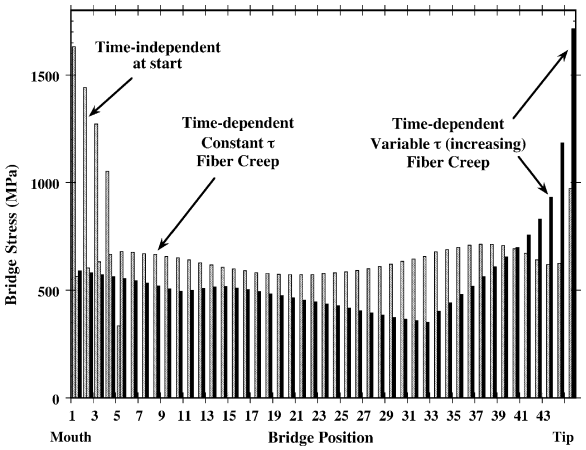

Fig. 6. Plot of bridging fiber stresses as a function of position in crack-wake bridging zone and under the assumptions of constant or variable sliding stress. The time-dependent data is after 2 years of crack growth.

3.3. Effect of fiber bridging forces

Shown in Fig. 6 is a plot of fiber-bridging stress as a function of bridge position within the crack wake for time-independent loading, fiber creep with a constant sliding stress, and fiber creep with variable sliding stress. The time-independent stress profile is greatly modified due to fiber creep, which results in stress relaxation of fibers near the crack mouth relative to fibers at the crack tip. Incorporation of the variable sliding stress results in reduced bridging stresses compared to the constant sliding stress case and faster initial crack growth. With increasing dose, however, fiber-bridging stresses begin to increase rapidly compared to lower dose or compared to the constant sliding stress case. Although this acts to reduce the crack growth rate it may signify an impending problem with fiber failures with increasing dose if fiber fracture strengths are attained.

4. Conclusions

The results of two different models that are linked with a common parameter, the fiber sliding stress, τ, have been combined to the great benefit of the dynamic crack growth model, which was lacking detail for the does-dependence of τ. Incorporating swelling data from two types of pyrocarbons, HDIC and LDIC, predicts that HDIC performs slightly better compared to LDIC as a fiber–matrix interface material. Pyrocarbon

swelling, however, is problematic and results in faster initial crack velocities but slower growth rates at higher doses. The reduced crack velocity is encouraging but results in higher than expected fiber stresses as the sliding stress increases with increasing dose. This may argue against the use of pyrocarbon interfaces for fusion reactor environments if fiber stresses approach fiber fracture strengths. However, the fast crack growth rates due to irradiation creep of SiC fine-grained fibers may be of more concern.

References

[1] L.L. Snead, T. Inoki, Y. Katoh, T. Taguchi, R.H. Jones, A. Kohyama, N. Igawa, Adv. Sci. Technol. 33 (2003) 129 (10th International Ceramics Congress 2002, Part D).
[2] C.M. Warwick, T.W. Clyne, J. Mater. Sci. 26 (1991) 3817.
[3] Y. Mikata, M. Taya, J. Compos. Mater. 19 (1985) 554.
[4] M. Kuntz, B. Meier, G. Grathwohl, J. Am. Ceram. Soc. 76 (1993) 2607.
[5] C.H. Henager, E.A. Le, R.H. Jones, J. Nucl. Mater. 329–333 (2004) 502.
[6] C.H. Henager, C.A. Lewinsohn, R.H. Jones, Acta Mater. 49 (2001) 3727.
[7] C.H. Henager Jr., R.G. Hoagland, Acta Mater. 49 (2001) 3739.
[8] R.H. Jones, C.H. Henager Jr., J. Eur. Ceram. Soc. 25 (2005) 1717.
[9] J.L. Kaae, Nucl. Technol. 35 (1977) 359.
[10] H.L. Heinisch, L.R. Greenwood, W.J. Weber, R.E. Williford, J. Nucl. Mater. 327 (2004) 175.
[11] D.K. Shetty, J. Am. Ceram. Soc. 71 (1988) 107.
[12] T.A. Parthasarathy, R.J. Kerans, J. Am. Ceram. Soc. 80 (1997) 2043.
[13] C.H. Henager Jr., R.H. Jones, C.F. Windisch Jr., M.M. Stackpoole, R. Bordia, Metall. Mater. Trans. A 27A (1996) 839.
[14] C.H. Henager Jr., R.H. Jones, J. Am. Ceram. Soc. 77 (1994) 2381.
[15] C.H. Henager Jr., R.H. Jones, Mater. Sci. Eng. A A166 (1993) 211.
[16] R. Scholz, G.E. Youngblood, J. Nucl. Mater. 283–287 (2000) 372.
[17] H. Ichikawa, Ann. Chim. Sci. Mater. 25 (2000) 523.
[18] T. Nozawa, Y. Katoh, L.L. Snead, Interfacial shear properties of silicon carbide composites with multi-layered interface, Fusion Semiannual Report DOE/ER-0313/38, June 30, 2005, Oak Ridge National Laboratory, p. 40.